

Linear Stability of a Combined Convective Flow in an Annulus

Armands Gritsans ¹, Valentina Koliskina ², Andrei Kolyshkin ^{2,*} and Felix Sadyrbaev ³

¹ Department of Physics and Mathematics, Daugavpils University, LV-5401 Daugavpils, Latvia; armands.gricans@du.lv

² Institute of Applied Mathematics, Riga Technical University, Zunda Embankment 10, LV-1048 Riga, Latvia; valentina.koliskina@rtu.lv

³ Institute of Mathematics and Computer Science, University of Latvia, LV-1459 Riga, Latvia

* Correspondence: andrejs.koliskins@rtu.lv

Abstract: Linear stability analysis of a combined convective flow in an annulus is performed in the paper. The base flow is generated by two factors: (a) different constant wall temperatures and (b) heat release as a result of a chemical reaction that takes place in the fluid. The nonlinear boundary value problem for the distribution of the base flow temperature is analyzed using bifurcation analysis. The linear stability problem is solved numerically using a collocation method. Two separate cases are considered: Case 1 (non-zero different constant wall temperatures) and Case 2 (zero wall temperatures). Numerical calculations show that the development of instability is different for Cases 1 and 2. Multiple minima on the marginal stability curves are found for Case 1 as the Prandtl number increases. Concurrence between local minima leads to the selection of the global minimum in such a way that a finite jump in the value of the wave number is observed for some values of the Prandtl number. All marginal stability curves for Case 2 have one minimum in the range of the Prandtl numbers considered. The corresponding critical values of the Grashof number decrease monotonically as the Prandtl number grows.

Keywords: linear stability; convective flow; bifurcation analysis; collocation method



Citation: Gritsans, A.; Koliskina, V.; Kolyshkin, A.; Sadyrbaev, F. Linear Stability of a Combined Convective Flow in an Annulus. *Fluids* **2023**, *8*, 130. <https://doi.org/10.3390/fluids8040130>

Academic Editors: Sergey Smolentsev and D. Andrew S. Rees

Received: 10 March 2023

Revised: 10 April 2023

Accepted: 11 April 2023

Published: 13 April 2023



Copyright: © 2023 by the authors. Licensee MDPI, Basel, Switzerland. This article is an open access article distributed under the terms and conditions of the Creative Commons Attribution (CC BY) license (<https://creativecommons.org/licenses/by/4.0/>).

1. Introduction

Temperature gradients can arise in a fluid as a result of the presence of internal heat sources. The density of heat sources can be constant, depending on one or several spatial coordinates, or can be a nonlinear function of the temperature. Examples include, but are not limited to, neutron irradiation in thermonuclear reactors [1], biomass thermal conversion [2,3], and convection in the Earth's mantle [4]. These examples also represent multiphysics problems where different physical mechanisms are coupled. There are three different approaches to the solution of complex problems in science and engineering: (a) experimental studies, (b) numerical modeling, and (c) stability analysis. Stability theory is used in an attempt to answer the question: when and how does the given base flow become unstable? Tools and methods of stability analysis are varied, ranging from stochastic analysis [5] to a deterministic approach [6] based on Lyapunov theory [7]. In the present paper we use a linear stability approach to analyze a convective flow in the region bounded by two vertical coaxial cylinders.

Hydrodynamic instability of a flow results in either a new laminar flow with more complicated structure (as for the case of the Taylor–Couette flow between two rotating cylinders [8]) or a rapid transition to turbulence (examples include, but are not limited to, pipe Poiseuille flow [9] or rapidly accelerated and decelerated pipe flows [10]). In applications for aerodynamics (stability of a flight of an airplane) or for hydraulic engineering (waterhammer phenomenon in rapidly decelerating flows) instability should be avoided or, at least, controlled. There are applications, however, where instability is desirable. One example of such a situation is biomass thermal conversion [2] where thermal instability

results in more intensive mixing and, possibly, more efficient energy conversion. Our objective in the present paper is to analyze the factors that may enhance instability.

The linear stability of a convective flow in a plane vertical channel caused by internal heat sources with constant density is analyzed in [11]. It is shown in [11] that depending on the value of the Prandtl number, two types of instability exist: (a) shear instability and (b) buoyant instability. Similar results are obtained later in [12]. The effect of different boundary conditions for the temperature on the stability characteristics is explored in [13]. Stability analysis of convective flows with constant density of heat sources in cylindrical geometry is conducted in [14–16]. The calculated linear stability characteristics are compared with experimental data in [16] for the case of heat sources of constant density in a pipe. Reasonable agreement is found in terms of the form of unstable perturbation and critical values of the Grashof number. Linear stability of a combined flow caused by external pressure gradient, uniform volumetric heating, and different constant wall temperatures in a vertical fluid layer are analyzed in [17]. Multiple local minima observed on the marginal stability curves facilitate instability.

As mentioned above, different forms of the distribution of heat sources are of interest in applications. One example is related to the flow where a light beam is passing through the fluid in such a way that all absorbed energy is released in the form of heat [18]. In this case the density of heat sources is an exponential function of the transverse coordinate. Such a distribution of heat sources is recently analyzed in [19] for the purpose of designing water-flow building facades with the objective to obtain solar energy. Other examples of flows with non-uniform density of heat sources are considered in [20–22].

Identification and use of new sources of energy are crucial for the development of our society. One promising alternative to classical sources of energy is biomass thermal conversion [23–25]. Since the problem includes different physical effects (chemical reactions, convection) and the corresponding models contain many parameters (see, for example, [26]), numerical modeling can be time-consuming. Linear stability analysis can be used as an alternative to numerical or experimental investigations in an attempt to identify the factors that affect the conversion process. Linear stability analyses of chemically reacting fluid are conducted in [27]. It is assumed in [26,27] that the density of internal heat sources is a nonlinear function of the temperature. This fact introduces an additional challenge for the base flow solution—the corresponding boundary value problem becomes nonlinear with one, two, or no solutions (depending on the value of the parameter that characterizes the thermal effect of the chemical reaction). Linear stability analysis is usually performed for the parameter range corresponding to two solutions. Thus, the “correct” base flow solution should be selected for stability analysis.

The study performed in the present paper is different from the other linear stability studies of a chemically reacting fluid in the following aspects: (a) bifurcation analysis is performed to identify the number of solutions of the nonlinear boundary value problem for the base flow temperature distribution and its structure; (b) the results from part (a) are used to choose the corresponding base flow solution for linear stability analysis; (c) convection is generated by two factors—internal heating of the fluid as a result of the chemical reaction and temperature difference between the walls; (d) it is found that the temperature gradient due to the difference between the wall’s temperatures is an additional destabilizing factor; (e) a new instability mode has been observed for $Pr = 7$. The paper is organized as follows. Mathematical formulation of the problem is presented in Section 2. Bifurcation analysis for the nonlinear boundary value problem is performed in Section 3 with the objective to identify the structure and number of solutions in the parameter space. Results from Section 3 are used to select the base flow solution. The linear stability problem for the base flow is formulated in Section 4. Numerical results of linear stability calculations for different values of the parameters of the problem are presented in Section 5. In addition, two cases are considered where the wall temperatures are either equal to zero or not.

2. Mathematical Formulation of the Problem

Consider a flow of a viscous incompressible fluid in the region $D = \{R_1 < \tilde{r} < R_2, 0 \leq \varphi < 2\pi, -\infty < \tilde{z} < +\infty\}$ between two concentric cylinders (see Figure 1). Linear stability analysis of the base flow (the base flow velocity distribution is shown in Figure 1 in red) is performed in the paper. The system of cylindrical polar coordinates $(\tilde{r}, \varphi, \tilde{z})$ with the origin at the axes of the cylinders is used to describe the flow. The following convention is used throughout: the variables with tildes are dimensional while the variables without tildes are dimensionless.

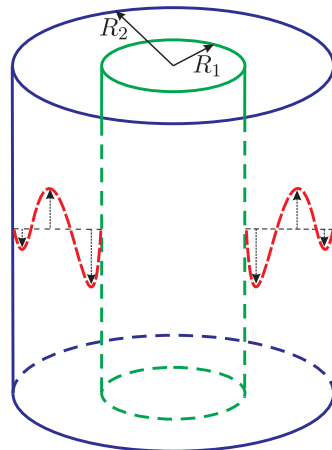


Figure 1. Sketch of the domain of the flow. The base flow velocity is shown in red.

Convective flow in the annulus formed by the cylinders is caused by two factors: (a) different constant temperatures $\pm T_0$ of the walls $r = R$ and $r = 1$, respectively, that cause a temperature gradient in the radial direction and (b) heat release due to chemical reaction that takes place in the fluid. Internal heat sources generate convection in the vertical direction. Here $R = R_1/R_2, r = \tilde{r}/R_2$. The distribution of the density of the heat sources follows the Arrhenius’ law [28]:

$$Q = Q_0 e^{-E/(R_0 \tilde{T})}. \tag{1}$$

The notations are as follows: E is the activation energy, R_0 is the universal gas constant, Q_0 is a constant, and \tilde{T} is the absolute temperature. The dimensionless form of the system of the Navier–Stokes equations under the Boussinesq approximation is used in the analysis:

$$\frac{\partial \mathbf{v}}{\partial t} + Gr(\mathbf{v} \cdot \nabla) \mathbf{v} = \nabla p + \Delta \mathbf{v} + T \mathbf{e}_k, \tag{2}$$

$$\frac{\partial T}{\partial t} + Gr \mathbf{v} \cdot \nabla T = \frac{1}{Pr} \Delta T + \frac{F}{Pr} e^T, \tag{3}$$

$$\nabla \cdot \mathbf{v} = 0. \tag{4}$$

The Boussinesq approximation is explained in detail in many papers (see, for example, [29–33]). The main assumptions are (a) non-uniformity of fluid density caused by changes in pressure is small and is neglected, (b) non-uniformity of density caused by non-uniform temperature distribution is assumed to be small, so that the density is given by

$$\tilde{\rho} = \rho(1 - \beta \tilde{T}), \tag{5}$$

where ρ is a constant and β is the coefficient of the thermal expansion. The detailed derivation of the dimensionless form of Equations (2)–(4) is found elsewhere (see, for example, [32]) and is not shown here for brevity. Here \mathbf{v} is the velocity of the fluid, T is the temperature, p is the pressure, and $\mathbf{e}_k = (0, 0, 1)$. To simplify the mathematical formulation of the source term we use the Frank-Kamenetskii transformation [28]. The transformation

consists of the following steps: (a) expand the exponent in a Taylor series in (1) and (b) keep only the linear terms of the expansion. As a result, a more convenient form of the source term is obtained (see (3)). Such a transformation is rather accurate for the range of parameters of interest in (1), see [28,34].

Some chemical reactions taking place in a fluid lead to heat generation and to formation of a product which has density different from the density of a reagent. Changes in the density caused by the changes in temperature and concentration lead to convection in the reacting fluid. Different formulations of the problem are available depending on the type of a chemical reaction or on the relative role of the thermal effect of the reaction. If the thermal effect for the reaction is large, one can neglect the dependence of internal heat generation from the concentration of the reagent. In this case, convection occurs due to internal heat sources distributed in the fluid in accordance with (1). This is the assumption considered in the present paper.

To transform the system of the Navier–Stokes equations with convection to the dimensionless form we choose the following scales, respectively, for length, $h = R_2$, time, h^2/ν , velocity, $g\beta^2 h R_0 T_0^2 / (\nu E)$, temperature, $R_0 T_0^2 / E$, and pressure, $\rho g \beta h R_0 T_0^2 / E$. Here ρ is the density of the fluid, g is the acceleration due to gravity, and ν is the viscosity of the fluid. The following dimensionless parameters are introduced: the Grashof number, $Gr = g\beta R_0 T_0^2 h^3 / (\nu^2 E)$, the Prandtl number, $Pr = \nu / \kappa$, and the Frank-Kamenetskii parameter, $F = [(Q_0 E h^2) / (\kappa R_0 T_0^2)] \exp[-E / (R_0 T_0)]$, where κ is the thermal diffusivity. The meaning of the dimensionless parameters is as follows. The Grashof number represents the ratio between the buoyancy force (due to non-uniformity in the temperature) and viscous force. The Prandtl number characterizes the properties of the fluid (the ratio of the viscosity and thermal conductivity). Finally, the Frank-Kamenetskii parameter represents internal heating of the fluid due to the chemical reaction that takes place in it. There exists a steady solution of (2)–(4) of the following structure:

$$\mathbf{v}_0 = (0, 0, W_0(r)), \quad T_0 = T_0(r), \quad p_0 = p_0(z). \tag{6}$$

The flow (6) is known as the fully developed flow in the literature [35]. It can be implemented in a middle portion of a sufficiently tall vertical annulus with a large aspect ratio. One example of the comparison of the linear stability characteristics with experimental data for aspect ratio of 38.6 is given in [36] where it is shown, in particular, that the measured wavelength of the cells is in good agreement with theoretical predictions obtained for an annulus of infinite length. Steady-state equations for the functions $W_0(r)$, $T_0(r)$, and $p_0(z)$ are obtained from (2)–(6) and have the form

$$W_0'' + \frac{W_0'}{r} + T_0 = C, \tag{7}$$

$$T_0'' + \frac{T_0'}{r} + Fe^{T_0} = 0, \tag{8}$$

where $C = dp_0/dz$.

The boundary conditions are

$$W_0(R) = 0, \quad W_0(1) = 0, \quad T_0(R) = -1, \quad T_0(1) = 1. \tag{9}$$

We assume that there are lids that cover the annulus at $\pm\infty$ so that

$$\int_R^1 r W_0(r) dr = 0. \tag{10}$$

Nonlinearity in the boundary value problem (7)–(10) appears only in the heat Equation (8). Bifurcation analysis performed in the next section shows that the number of solutions of the problem (8) and (9) for the temperature $T_0(r)$ depends on the value of the Frank-Kamenetskii parameter F .

3. Bifurcation Analysis

Consider the boundary value problem

$$T_0''(r) + \frac{T_0'(r)}{r} + Fe^{T_0(r)} = 0, \tag{11}$$

$$T_0(R) = -1, \quad T_0(1) = 1, \tag{12}$$

where $F > 0$ and $0 < R < 1$. Let us consider the auxiliary initial value problem (11),

$$T_0(1) = 1, \quad T_0'(1) = \beta. \tag{13}$$

Acting in a similar way as in [37,38], the change of variables $r = e^{-\tau}$, $T_0(r) = w(\tau) + 2\tau$ reduces (11), (13) to the initial value problem

$$w''(\tau) + Fe^{w(\tau)} = 0, \quad w(0) = 1, \quad w'(0) = -2 - \beta. \tag{14}$$

By calculations, the function

$$w(\tau) = \ln \frac{4e^{1+\tau\sqrt{(2+\beta)^2+2Fe}}((2+\beta)^2+2Fe)}{\left[-2-\beta+\sqrt{(2+\beta)^2+2Fe}+(2+\beta+\sqrt{(2+\beta)^2+2Fe})e^{\tau\sqrt{(2+\beta)^2+2Fe}}\right]^2}$$

solves (14) in the interval $(-\infty, +\infty)$, and thus the function

$$T_0(r) = \ln \frac{4er^{-2+\sqrt{(2+\beta)^2+2Fe}}((2+\beta)^2+2Fe)}{\left[2+\beta+\sqrt{(2+\beta)^2+2Fe}+(-2-\beta+\sqrt{(2+\beta)^2+2Fe})r\sqrt{(2+\beta)^2+2Fe}\right]^2} \tag{15}$$

solves (11), (13) in the interval $(0, +\infty)$.

Let R be a fixed number in the interval $(0, 1)$. Suppose that a function $T_0(r)$ is defined by (15); then, the equation $T_0(R) = -1$ defines the bifurcation curve Γ_R in the (F, β) -plane, which determines all solutions to (11), (12). We see that $T_0(R) = -1$ if and only if $G_R(F, \beta) = 0$, where

$$G_R(F, \beta) := 4e^2R^{-2+\sqrt{(2+\beta)^2+2Fe}}((2+\beta)^2+2Fe) - \left[2+\beta+\sqrt{(2+\beta)^2+2Fe}+(-2-\beta+\sqrt{(2+\beta)^2+2Fe})R\sqrt{(2+\beta)^2+2Fe}\right]^2.$$

Hence, $\Gamma_R = \{(F, \beta) \in \mathbb{R}^2 : F > 0, \beta \in \mathbb{R}, G_R(F, \beta) = 0\}$. By numerical analysis, the curve Γ_R is \supset -shaped and has a turning point (F^*, β^*) from right to left. Thereby, (11), (12) has exactly two solutions if $F \in (0, F^*)$, exactly one solution if $F = F^*$, and has no solutions if $F > F^*$.

In Figure 2, the bifurcation curve Γ_R is depicted for $R = 0.5$. The vertical straight line $F = 8$ and the curve Γ_R intersect at the points $P_1 = (8, -12.238)$ and $P_2 = (8, -1.4237)$; the point $P^* = (10.847, -6.3181)$ is a turning point of Γ_R . In Figure 3, three solutions of (11), (12) are presented: the green solution corresponds to the point P_1 , the blue solution corresponds to the point P_2 , and the brown solution corresponds to the point P^* . In Figure 4, the bifurcations curves Γ_R and their turning points are depicted if $R = 0.1i, i \in \{1, 2, \dots, 8\}$. In Figure 5, the dependence of F^* on R is presented for $R = 0.1j, j \in \{1, 2, \dots, 9\}$, where (F^*, β^*) is a turning point of Γ_R .

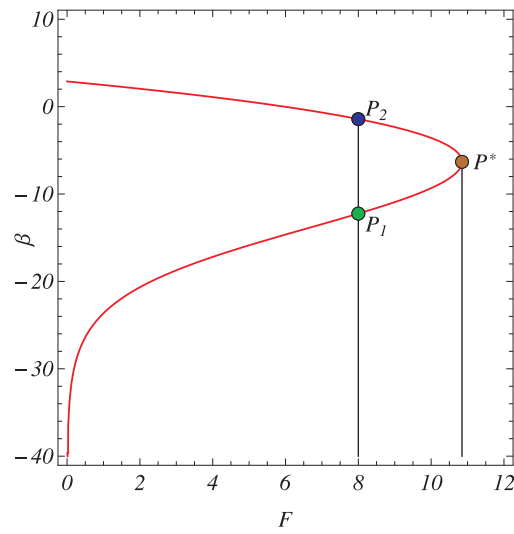


Figure 2. The curve Γ_R for $R = 0.5$.

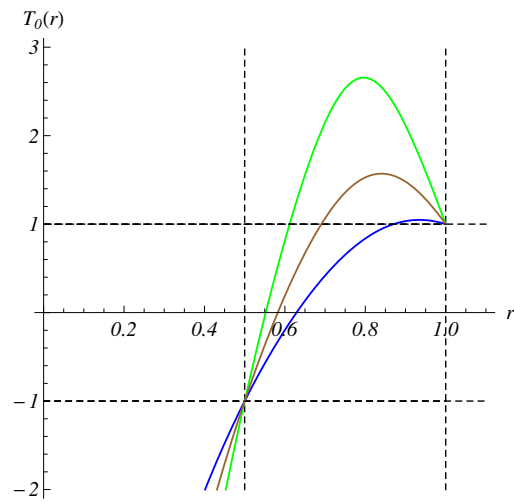


Figure 3. Three solutions of (11), (12) for $R = 0.5$.

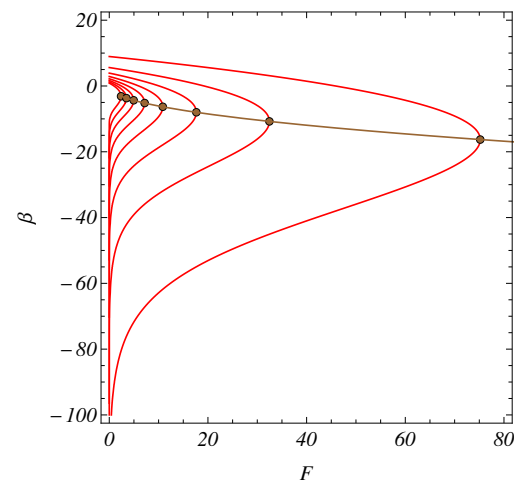


Figure 4. Evolution of the curves Γ_R for $R = 0.1j, j \in \{1, 2, \dots, 9\}$.

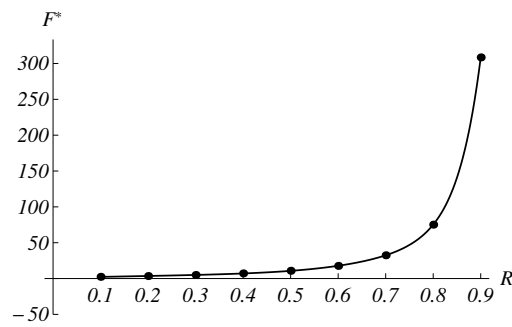


Figure 5. The dependence of F^* on R .

4. Linear Stability Analysis

Bifurcation analysis conducted in the previous section allows one to determine (for each R) the range of values of F for which there exists a steady solution of (11) and (12), namely, $0 < F < F^*$, where F^* is given by Figure 5. In addition, it helps to select the base flow temperature distribution (the physically realizable solution is shown in Figure 3 in blue and has the smallest norm).

Consider a perturbed flow of the form

$$\begin{aligned}
 \mathbf{v}(r, z, t) &= \mathbf{u}(r) e^{-\lambda t + ikz}, \\
 T(r, z, t) &= \theta(r) e^{-\lambda t + ikz}, \\
 p(r, z, t) &= q(r) e^{\lambda t + ikz},
 \end{aligned}
 \tag{16}$$

where $\mathbf{u}(r) = (u(r), 0, w(r))$, k is the wave number, and $\lambda = \lambda_r + i\lambda_i$ is a complex eigenvalue. Base flow (6) is said to be linearly stable if all $\lambda_r > 0$, and linearly unstable, if at least one $\lambda_r < 0$. Previous studies [39] have shown that the most unstable perturbation is axisymmetric for relatively small gaps (including the case $R = 0.7$ considered in the present paper) so that we restrict ourselves to axisymmetric perturbations. Substituting (16) into (2)–(4) we obtain

$$u'' + \frac{u'}{r} - k^2 u - \frac{u}{r^2} = q' + ikGrkuW_0 - \lambda u,
 \tag{17}$$

$$w'' + \frac{w'}{r} - k^2 w + \theta = ikq + iGr(uW_0' + ik\theta W_0) - \lambda w,
 \tag{18}$$

$$\frac{1}{Pr}(\theta'' + \frac{\theta'}{r} - k^2\theta + e^{T_0}\theta) = Gr(uT_0' + ik\theta W_0) - \lambda\theta,
 \tag{19}$$

$$u' + \frac{u}{r} + ikw = 0.
 \tag{20}$$

The boundary conditions are

$$u(R) = 0, \quad u(1) = 0, \quad w(R) = 0, \quad w(1) = 0, \quad \theta(R) = 0, \quad \theta(1) = 0.
 \tag{21}$$

Equations (17), (18) and (20) are transformed to one ordinary differential equation of order four by eliminating q and w from (17), (18) and (20). The obtained equation is coupled with (19). In addition, two extra boundary conditions for the function u are required:

$$u'(R) = 0, \quad u'(1) = 0.
 \tag{22}$$

Conditions (22) follow from (20) and (21). The functions $u(\xi)$ and $\theta(\xi)$ for the corresponding boundary value problem are approximated as follows:

$$u(\xi) = \sum_{n=0}^N a_n(1 - \xi^2)^2 T_n(\xi), \quad \theta(\xi) = \sum_{n=0}^N b_n(1 - \xi^2) T_n(\xi),
 \tag{23}$$

where $\xi = 2r/(1 - R) - (1 + R)/(1 - R)$ and $T_n(\xi)$ is the Chebyshev polynomial of the first kind. The collocation method is used to discretize the obtained problem where the collocation points are

$$\xi_j = \cos(\pi j/N), \quad j = 0, 1, \dots, N. \tag{24}$$

The discretized generalized eigenvalue problem is solved using Matlab routine *eig*.

5. Numerical Results

Calculations are performed for the following two cases: (a) nonzero boundary conditions (9) for the function $T_0(r)$ and (b) zero boundary conditions for the temperature $T_0(r)$. We refer to cases (a) and (b) in the paper as Case 1 and Case 2, respectively. The values of the Prandtl number that are chosen for calculations ($0 < Pr < 15$) correspond to different types of fluids. In particular, gases usually have the Prandtl number of order 0.7. Larger values of the Prandtl number (from 3 to 15) may correspond to biomass slurry that is typically present during the process of energy recovery from wet waste biomass, as is shown in [40]. Figures 6–9 plot marginal stability curves for four values of the Prandtl number and three values of the Frank-Kamenetskii parameter F (Case 1 with unequal wall temperatures). The stability region is below the curves.

It can be seen from Figures 6–9 that the increase in Pr is associated with continuous deformation of the marginal stability curves. For small Prandtl numbers ($Pr = 0.79$ and $Pr = 3$ in Figures 6 and 7) all eigenvalues have positive real parts below the curves and negative real parts above the curves, respectively. On the marginal stability curves in Figures 6 and 7 one eigenvalue has a zero real part. As the Prandtl number grows, other eigenvalues may become unstable for a certain range of k while the eigenvalue that was previously unstable may become stable. The appearance of new unstable eigenvalues results in the sharp change of the marginal stability curve and the appearance of additional minima on the marginal stability curves. Note that the second and third minimum appears on the curves for $Pr = 5$ and $Pr = 7$, respectively.

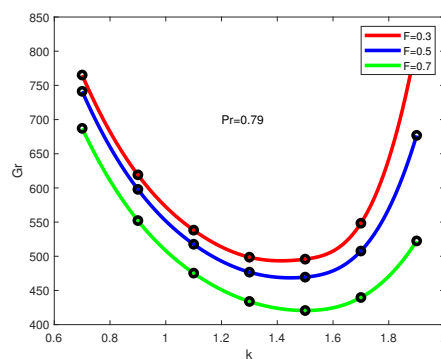


Figure 6. Marginal stability curves for $Pr = 0.79$ (Case 1).

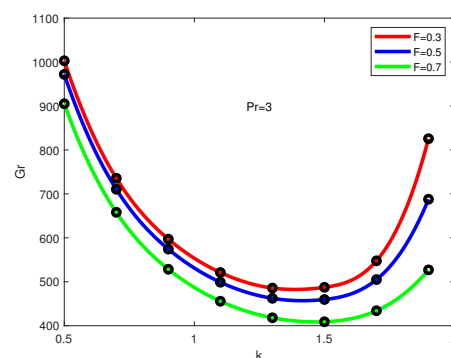


Figure 7. Marginal stability curves for $Pr = 3$ (Case 1).

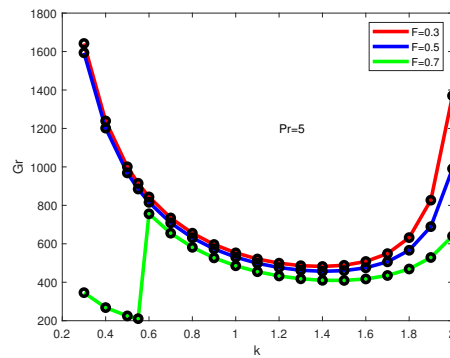


Figure 8. Marginal stability curves for $Pr = 5$ (Case 1).

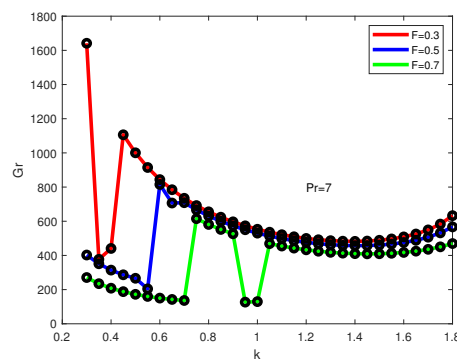


Figure 9. Marginal stability curves for $Pr = 7$ (Case 1).

Previous studies [11,15,17,41] have shown that for large Pr marginal stability curves can have multiple loops where the base flow is unstable with respect to several modes. Our objective is not to provide detailed description of the marginal stability curves, but to determine the values of the parameters that correspond to the absolute minimum on the marginal stability curve. As a result, we provide only envelopes of the marginal stability curves shown in Figures 6–9.

Similar calculations are performed for Case 2 (zero wall temperatures for the function $T_0(r)$). The results are shown in Figures 10–13. Comparing Figures 6–9 with Figures 10–13, we see that there is no deformation of the marginal stability curves for Case 2: all curves have one minimum.

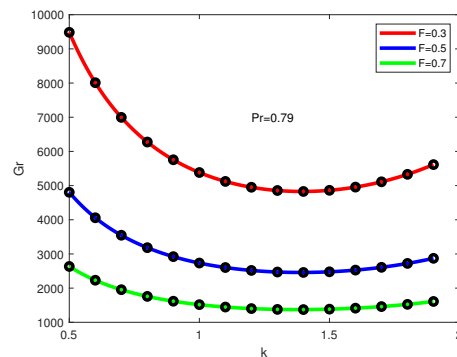


Figure 10. Marginal stability curves for $Pr = 0.79$ (Case 2).

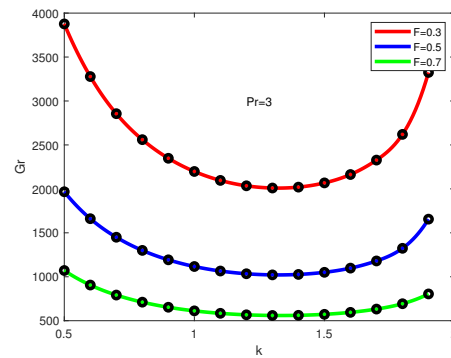


Figure 11. Marginal stability curves for $Pr = 3$ (Case 2).

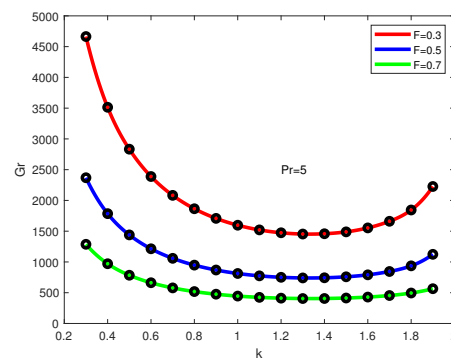


Figure 12. Marginal stability curves for $Pr = 5$ (Case 2).

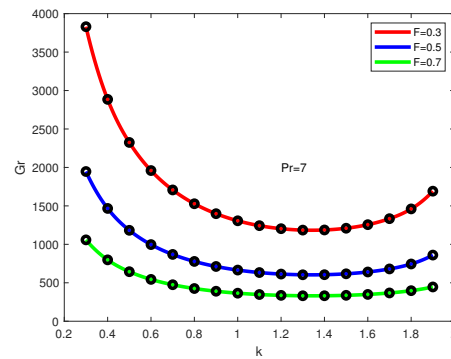


Figure 13. Marginal stability curves for $Pr = 7$ (case 2).

The critical Grashof numbers $Gr_c = \min_k Gr$ and the corresponding critical wave numbers k_c are shown in Figures 14 and 15, respectively. The “elbows” for the curves in Figure 14 represent the change of the form of instability (see Figures 8 and 9): the minimum that appears in the region of smaller k as Pr increases is further lowered as Pr continues to increase. The second minimum (at $k \approx 1.4$) is not so sensitive to the change in Pr (see Figures 8 and 9). Eventually the two minima coincide: calculations show that for $F = 0.3$ we have two equal minima ($Gr_c = 482.9$ at $k = 1.39$ and $k = 0.4$). A further increase in Pr leads to the critical Grashof numbers in the region of smaller k . As a result, one has a finite jump from $k = 1.39$ to $k = 0.4$ (see Figure 15) and the critical Grashof numbers start to decrease. Similar changes in Gr_c and k_c take place also for $F = 0.5$ and $F = 0.7$. The appearance of the third minimum on the marginal stability curve (see Figure 9) leads to another jump in k for the cases $F = 0.5$ and $F = 0.7$.

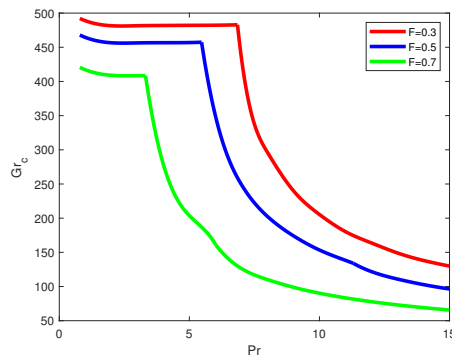


Figure 14. Critical Grashof numbers versus Pr for Case 1.

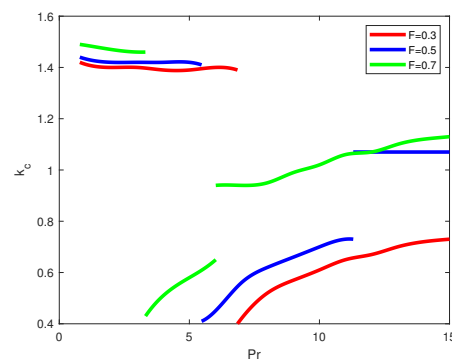


Figure 15. Critical wave numbers versus Pr for Case 1.

Critical values of the Grashof number and the corresponding critical wave numbers are shown in Figures 16 and 17 for Case 2 (zero wall temperatures). Comparing Figures 14 and 15 for Case 1 with the corresponding Figures 16 and 17 for Case 2, we see different behavior of the instability modes. The critical values of the Grashof number for Case 2 decrease monotonically as Pr grows, and the critical wave numbers do not change much in the range of the Prandtl numbers considered: $0 < Pr \leq 15$. In contrast, for Case 1 there is a “plato” phase for each F where the critical Grashof numbers do not change. Further increase in Pr leads to a decrease of the critical Grashof numbers.

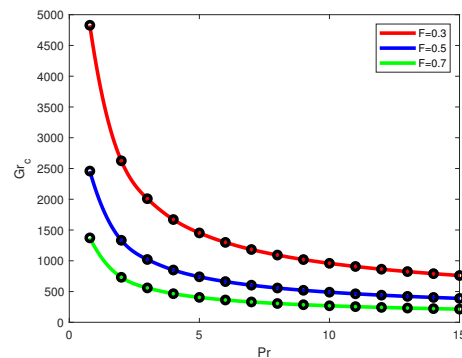


Figure 16. Critical Grashof numbers versus Pr for Case 2.

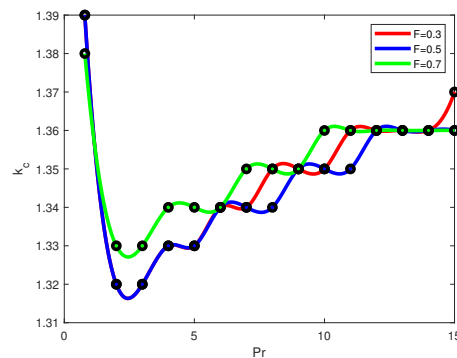


Figure 17. Critical wave numbers versus Pr for Case 2.

6. Discussion

Linear stability analysis of a steady convective flow caused by two factors: (a) internal heat generation as the result of a chemical reaction and (b) different constant wall temperatures is analyzed in this paper. The flow is considered in a vertical annular fluid layer under the assumption that the total fluid flux through the cross-section of the layer is equal to zero. The corresponding boundary value problem for the heat equation is nonlinear. Bifurcation analysis is performed in the paper to identify the number of solutions of the boundary value problem depending on the value of the Frank-Kamenetskii parameter, representing the intensity of heat release as a result of the chemical reaction. In addition, solutions to the nonlinear boundary value problem are also obtained. The goal of the bifurcation analysis is to select the correct form of the base flow solution.

The linear stability problem is solved numerically using a collocation method. Two cases are considered separately: Case 1 (different constant wall temperatures) and Case 2 (zero wall temperatures). Calculations show that linear stability characteristics differ considerably between Case 1 and Case 2. In Case 1, multiple minima of the marginal stability curves are observed as the Prandtl number increases. Depending on the relative values of the local minima, the global minimum can be associated with different wave numbers. As a result, finite jumps in wave numbers are observed as the Prandtl number increases. Critical Grashof numbers almost do not change in the interval $0 < Pr < \hat{Pr}$, where \hat{Pr} depends on the Frank-Kamenetskii parameter F . In the region $Pr > \hat{Pr}$ the critical Grashof numbers decrease monotonically as the Prandtl number increases. Marginal stability curves for Case 2 have one minimum in the range of the Prandtl numbers considered, $0 < Pr \leq 15$, and the corresponding wave numbers do not change much. The results show that instability is mainly of hydrodynamical nature for small Prandtl numbers considered in the paper ($Pr = 0.79$). It occurs due to the presence of inflection points in the base flow velocity profile. As the Prandtl number increases, new modes of instability appear; thermal factors are playing a more important role. The appearance of the new modes is seen from the marginal stability curves where one or two additional minima are observed as the Prandtl number grows. Thus, either shear or buoyant instability takes place depending on the value of the Prandtl number.

In order to analyze the development of instability in the region of the parameter space where the flow becomes linearly unstable weakly nonlinear theory can be considered. The approach is based on the use of a multiple scale method where the expansion is constructed in the neighborhood of the critical point (k_c, Gr_c, λ_c) . It is assumed that the Grashof number is slightly above the critical value so that the flow is unstable but the growth rate of the unstable perturbation is small. The result is an amplitude evolution equation for the most unstable mode (such as the complex Ginzburg–Landau Equation [42]). Weakly nonlinear models were successfully used in the past to investigate instability above the threshold for Taylor–Couette flows [43] or shallow water flows [44]. The advantages of the weakly nonlinear method are as follows. First, the amplitude evolution equation is usually much simpler to deal with than the full nonlinear formulation of the problem. Second, some of

the amplitude equations can have a rich variety of solutions from deterministic to almost chaotic depending on the values of the parameters [42]. Third, previous studies have shown that amplitude evolution equations can be successfully used for a rather wide range in the parameter space, even if the multiple scale expansion is considered in a small neighborhood of the critical point. The authors are currently working on this topic.

Author Contributions: Conceptualization, A.G. and A.K.; methodology, A.G., V.K., A.K. and F.S.; software, A.G., V.K. and A.K.; validation, A.G., V.K. and A.K.; formal analysis, A.G., A.K. and F.S.; writing—original draft preparation, A.G., V.K., A.K. and F.S.; writing—review and editing, A.G., A.K. and F.S.; supervision, A.G. and A.K. All authors have read and agreed to the published version of the manuscript.

Funding: This research was funded by the Latvian Council of Science project No. lzp-2020/1-0076.

Data Availability Statement: The data that support the findings of this study are available from the corresponding author upon reasonable request.

Acknowledgments: The authors thank the editor and anonymous referees for their constructive comments, which helped us to improve the manuscript.

Conflicts of Interest: The authors declare no conflict of interest.

References

- Hudoba, A.; Molokov, S. Linear stability of buoyant convective flow in a vertical channel with internal heat sources and a transverse magnetic field. *Phys. Fluids* **2016**, *28*, 114103. [[CrossRef](#)]
- Lewandowski, W.M.; Ryms, M.; Kosakowski, W. Thermal biomass conversion: A review. *Processes* **2020**, *8*, 516. [[CrossRef](#)]
- Barmina, I.; Purmalis, M.; Valdmānis, R.; Zake, M. Electrodynamic control of the combustion characteristics and energy production. *Combust. Sci. Technol.* **2016**, *188*, 190–206. [[CrossRef](#)]
- Richard, Y. Physics of mantle convection. In *Treatise of Geophysics*; Elsevier: New York, NY, USA, 2015; Volume 7, pp. 23–71.
- Carkovs, J.; Matvejevs, A. Stochastic stability of pipeline induced by pulsed fluid flow. In Proceedings of the 15th Conference on Applied Mathematics Aplimat 2016, Bratislava, Slovakia, 2–4 February 2016; pp. 189–196.
- Drazin, P.G.; Reid, W.H. *Hydrodynamic Stability*, 2nd ed.; Cambridge University Press: Cambridge, UK, 2004.
- Lyapunov, A.M. The general problem of the stability of motion. *Int. J. Control* **1992**, *55*, 531–534. [[CrossRef](#)]
- Jones, C.A. The transition to wavy Taylor vortices. *J. Fluid Mech.* **1985**, *157*, 135–162. [[CrossRef](#)]
- Avila, M.; Barkley, D.; Hof, B. Transition to turbulence in pipe flow. *Annu. Rev. Fluid Mech.* **2023**, *55*, 575–602. [[CrossRef](#)]
- Greenblatt, D.; Moss, E.A. Rapid transition to turbulence in pipe flows accelerated from rest. *J. Fluid Eng.* **2003**, *125*, 1072–1075. [[CrossRef](#)]
- Gershuni, G.Z.; Zhukhovitskii, E.M.; Iakimov, A.A. Two kinds of instability of stationary convective motion induced by internal heat sources. *J. Appl. Math. Mech.* **1973**, *37*, 544–548. [[CrossRef](#)]
- Takashima, M. The stability of natural convection in a vertical fluid layer with internal heat generation. *J. Phys. Soc. Jpn.* **1983**, *52*, 2364–2370. [[CrossRef](#)]
- Takashima, M. The stability of natural convection due to internal heat sources in a vertical fluid layer. *Fluid Dyn. Res.* **1990**, *6*, 15–23. [[CrossRef](#)]
- Rogers, B.B.; Yao, L.S. The importance of Prandtl number for mixed-convection instability. *Trans. ASME C J. Heat Transf.* **1993**, *115*, 482–486.
- Kolyshkin, A.A.; Vaillancourt, R. Stability of internally generated thermal convection in a tall vertical annulus. *Can. J. Phys.* **1991**, *69*, 743–748. [[CrossRef](#)]
- Kolyshkin, A.; Koliskina, V. Stability of a convective flow in a pipe caused by internal heat generation. *JP J. Heat Mass Transf.* **2018**, *15*, 515–530. [[CrossRef](#)]
- Shankar, B.M.; Kumar, J.; Shivakumara, I.S. Stability of mixed convection in a differentially heated vertical fluid layer with internal heat sources. *Fluid Dyn. Res.* **2019**, *51*, 055501. [[CrossRef](#)]
- Shikhov, V.M.; Yakushin, V.I. Stability of convective motion caused by inhomogeneously distributed internal heat sources. *Fluid Dyn.* **1977**, *12*, 457–461.
- Rashevski, M.; Slavtchev, S.; Stoyanova, M. Natural and mixed convection in a vertical water-flow chamber in the presence of solar radiation. *Eng. Sci. Technol.* **2022**, *33*, 10173. [[CrossRef](#)]
- Kolyshkin, A.A.; Vaillancourt, R. On the stability of convective motion caused by inhomogeneous heat sources. *Arab. J. Sci. Eng.* **1992**, *17*, 655–662. [[CrossRef](#)]
- Saravan, S.; Kandaswamy, P. Thermal instability of a nonuniformly heat generating annual fluid layer. *Int. J. Heat Mass Transf.* **2006**, *49*, 269–280.

22. Kolyshkin, A.; Koliskina, V.; Volodko, I.; Iltins, I. Convective instability of a steady flow in an annulus caused by internal heat generation. *Proc. Latv. Acad. Sci. Sect. B* **2020**, *74*, 293–298. [[CrossRef](#)]
23. Yamakawa, C.K.; Quin, F.; Mussatto, S.I. Advances and opportunities in biomass conversion technologies and biorefineries for the development of a bio-based economy. *Biomass Bioenergy* **2018**, *119*, 54–60. [[CrossRef](#)]
24. Nussbauer, T. Combustion and co-combustion of biomass: Fundamentals, technologies and primary measures for emission reduction. *Energy Fuels* **2003**, *17*, 1510–1521. [[CrossRef](#)]
25. Luo, Z.; Zhou, J. Thermal convection of biomass. In *Handbook of Climate Change Mitigation*; Springer: Berlin/Heidelberg, Germany, 2012; pp. 1001–1042. [[CrossRef](#)]
26. Kalis, H.; Marinaki, M.; Strautins, U.; Zake, M. On numerical simulation of electromagnetic field effects in the combustion process. *Math. Model. Anal.* **2018**, *23*, 327–343.
27. Eremin, E.A. On the stability of steady convective motion generated by internal heat sources. *Fluid Dyn.* **1983**, *18*, 438–441. [[CrossRef](#)]
28. Frank-Kamenetskii, D.A. *Diffusion and Heat Exchange in Chemical Kinetics*; Princeton: Princeton, NJ, USA, 1955. [[CrossRef](#)]
29. Boussinesq, J. *Théorie Analytique de la Chaleur*; Gauthier-Villars: Paris, France, 1903.
30. Spiegel, E.A.; Veronis, G. On the Boussinesq approximation for a compressible fluid. *Astrophys. J.* **1960**, *131*, 442–447.
31. Mihailjan, J.M. A rigorous exposition of the Boussinesq approximation applicable to a thin layer of fluid. *Astrophys. J.* **1962**, *136*, 1126–1133. [[CrossRef](#)]
32. Gershuni, G.Z.; Zhukhovitskii, E.M. *Convective Stability of Incompressible Fluids*; Ketter Publications: Jerusalem, Israel, 1976. [[CrossRef](#)]
33. Gray, D.D.; Giorgini, A. The validity of the Boussinesq approximation for liquids and gases. *Int. J. Heat Mass Transf.* **1976**, *19*, 545–551.
34. White, D., Jr.; Johns, L.E. The Frank-Kamenetskii transformation. *Chem. Eng. Sci.* **1987**, *42*, 1849–1851. [[CrossRef](#)]
35. Bachelor, G.K. *An Introduction to Fluid Dynamics*; Cambridge University Press: Cambridge, UK, 2000. [[CrossRef](#)]
36. Choi, I.G.; Corpela, S.A. Stability of the conduction regime of natural convection in a tall vertical annulus. *J. Fluid Mech.* **1980**, *99*, 725–738.
37. Bebernes, J.; Eberly, D. *Mathematical Problems from Combustion Theory*; Springer: New York, NY, USA, 1989. [[CrossRef](#)]
38. Gritsans, A.; Kolyshkin, A.; Ogorelova, D.; Sadyrbaev, F.; Samuilik, I.; Yermachenko, I. Solutions of nonlinear boundary value problem with applications to biomass thermal conversion. In Proceedings of the 20th International Scientific Conference “Engineering for Rural Development”, Jelgava, Latvia, 26–28 May 2021; pp. 837–842.
39. Iltins, I.; Iltina, M.; Kolyshkin, A.; Koliskina, V. Linear stability of a convective flow in an annulus with a nonlinear heat source. *JP J. Heat Mass Transfer.* **2019**, *18*, 315–329.
40. Noguchi, T.; Noda, Y.; Yamasaki, Y.; Inoue, S.; Kawai, Y.; Shimizu, Y.; Minowa, T.; Matsumura, Y. Heat transfer characteristics of biomass slurry under high pressure and high temperature. *J. Jpn. Inst. Energy* **2011**, *90*, 874–880. [[CrossRef](#)]
41. Wang, B.F.; Zhou, L.; Wan, Z.H.; Ma, D.J.; Sun, D.J. Stability analysis of Rayleigh-Benard convection in a cylinder with internal heat generation. *Phys. Rev. E* **2016**, *94*, 013108. [[CrossRef](#)]
42. Aranson, I.; Kramer, L. The world of the complex Ginzburg-Landau equation. *Rev. Mod. Phys.* **2002**, *74*, 99–143. [[CrossRef](#)]
43. Martinand, D.; Serre, E.; Lueptow, R.M. Linear and weakly nonlinear analyses of cylindrical Couette flow with axial and radial flows. *J. Fluid Mech.* **2017**, *824*, 438–476. [[CrossRef](#)]
44. Kolyshkin, A.A.; Ghidaoui, M.S. Stability analysis of shallow wake flows. *J. Fluid Mech.* **2003**, *494*, 355–377. [[CrossRef](#)]

Disclaimer/Publisher’s Note: The statements, opinions and data contained in all publications are solely those of the individual author(s) and contributor(s) and not of MDPI and/or the editor(s). MDPI and/or the editor(s) disclaim responsibility for any injury to people or property resulting from any ideas, methods, instructions or products referred to in the content.